Current-voltage characteristic and sheet resistances after annealing of femtosecond laser processed sulfur emitters for silicon solar cells

Thomas Gimpel,[1,a)] Kay-Michael Guenther,[2] Stefan Kontermann,[1] and Wolfgang Schade[1,2]
[1]*Fraunhofer Heinrich Hertz Institute (HHI), Am Stollen 19B, D-38640 Goslar, Germany*
[2]*Clausthal University of Technology, EFZN, Am Stollen 19B, D-38640 Goslar, Germany*

(Received 1 November 2013; accepted 26 July 2014; published online 5 August 2014)

The characteristics of laser doped sulfur emitters are strongly dependent on annealing processes. We show how annealing increases the efficiency of silicon solar cells with such an emitter. Sheet resistance analysis reveals that up to an annealing temperature of 400 °C the emitter sheet resistivity increases. A lower sulfur donor concentration is concluded, which likely occurs by means of sulfur diffusion and capturing of sulfur donors at intrinsic silicon defects. Above that temperature, the emitter sheet resistance decreases, which we find to originate from healing of laser induced structural defects involving traps within the depletion zone of the silicon pn-junction. © *2014 AIP Publishing LLC*. [http://dx.doi.org/10.1063/1.4892474]

Chalcogen-supersaturated silicon[1–4] features enhanced absorption below the silicon band gap[5] and simultaneous n-type doping of the silicon substrate.[3,6] Therefore, this substrate is highly attractive for novel optoelectronic devices like silicon infrared photodiodes[7–9] and intermediate band photovoltaic cells.[3,10] The chalcogens are impurities incorporated far above the solubility limit.[11,12] The required incorporation techniques diminish the silicon crystal quality,[11,13] leading to intrinsic defects in the silicon lattice. Subsequent thermal processes enhance among others the performance of a pn-junction with such a sulfur emitter.[6,11,14] Previous work investigates the temperature dependence of the infrared absorption of chalcogen doped silicon.[1,5,12,15–17] Changes in the infrared absorption are attributed to sulfur diffusion processes occurring at temperatures above $T = 300\,^{\circ}\mathrm{C}$.[18] An explanation for the improvement of a device performance as in Refs. 6 and 11 is not correlated by sulfur diffusion. On the other hand, annealing processes are investigated in correlation with structural changes in the silicon lattice.[12,13] It is found that annealing at $T = 800\,^{\circ}\mathrm{C}$ improves the crystal quality.[12,13] However, it remains still unclear if the impact of annealing influences the pn-junction. Obviously, both effects, sulfur diffusion and changes in the silicon lattice, play an important role in sulfur hyperdoped silicon emitter. This paper correlates those two effects with the influence on the sulfur emitter and therewith with the performance of a photovoltaic device. We analyze the *IV* characteristics of femtosecond laser sulfur hyperdoped pn-junctions and determine the sulfur emitter sheet resistances by the Transmission Line Model (TLM)[20–23] before and after annealing.

Silicon solar cells are manufactured on $20 \times 20\,\mathrm{mm}^2$ boron doped Si (100) substrates with a base resistivity of $1 - 5\,\Omega\mathrm{cm}$. The samples are sulfur hyperdoped and structured by femtosecond laser pulses from a 10 kHz regenerative amplifier system (Mantis seed laser from Coherent and Spitfire amplifier from Spectra Physics) at a wavelength of 800 nm. The laser repetition rate is lowered to 625 Hz and the fluency is set to $E \approx 2.0\,\mathrm{J/cm}^2$ at a measured laser spot diameter (intensity $1/e^2$) of $D \approx 80\,\mu\mathrm{m}$. Samples are scanned under the laser beam at a velocity of 10 mm/s with a line pitch of 55 μm in a sulfur hexafluoride (SF_6) ambient at a pressure of $p = 0.66$ bar. The lasered samples, manufactured to solar cells, are annealed in a tube furnace under 95/5 forming gas flow for $t = 20$ min at $T = 800\,^{\circ}\mathrm{C}$. The cooling process takes place at air ambient and takes about 3 min, while the sample is mounted on a thick silica boat. With this temperature regime, we expect the additional sub band gap absorption to vanish.[15] This is confirmed by absorption measurements on similar samples (not shown here). Furthermore, we see no influence from the forming gas flow through the furnace, since the cooling takes place at air ambient where potentially incorporated hydrogen is desorbed. The back contact of these solar cell samples consists of screen printed aluminum paste, fired in a separate tube furnace for $t = 2$ min at $T = 800\,^{\circ}\mathrm{C}$ and cooled as mentioned before. To avoid this temperature step for the non-annealed samples, the back contact on these samples is applied before the laser process. Front contacts are deposited by a photolithographical mask on the solar cell samples in a pulsed laser deposition chamber with a metal stack of titanium, palladium, and silver (30 nm, 30 nm, and 200 nm). Note that no solar cell device engineering like sealing and passivation of the roughened laser treated front surface or an additional phosphorus emitter is applied to any of the samples. This solar cell structure is distinguished by the fact that the sulfur emitter and the front surface structuring are performed within one laser process step only. The TLM samples feature a base resistivity of $12 - 15\,\Omega\mathrm{cm}$. The laser process is the same as applied to the solar cell samples. The TLM samples are annealed in air ambient at different temperatures and durations and no back contact is applied, as it is not necessary for the TLM measurements. The TLM samples possess several single front contact fingers consisting of the same metal stack as the solar cell samples. The TLM contacts are spread as wide as the sample and the distance between up to nine non-equidistant contact fingers is varied from 0.3 mm to 6.4 mm. Resistances between the fingers are measured via the four-point probe method and are plotted versus their

a)Author to whom correspondence should be addressed. Electronic mail: thomas.gimpel@hhi.fraunhofer.de. Telephone: +49 53216855118.

distances. The emitter sheet resistance can be extracted from the slope of this curve and determined quantitatively, when length and width of the fingers are known.

The solar cells are assessed by using the two diode model,[24] where a solar cell is modeled by an equivalent circuit with two diodes and a series and parallel resistance. Therewith, the behavior of base and emitter of the solar cell can be distinguished separately from mechanisms within the space charge region as well as from losses related to the series and parallel resistances. Solar cell parameters are obtained from measured *IV* curves and by fitting those with the free software IVFIT (version 2.12) using fixed ideality factors for the first ($n_1 = 1$) and the second ($n_2 = 2$) diode.[25] Fig. 1(a) shows the *IV* characteristics under AM 1.5 conditions at one sun illumination of $100\,\mathrm{mW/cm^2}$ and Fig. 1(b) reveals the dark *IV* characteristics for a non-annealed and an annealed solar cell sample. The corresponding *IV* curve parameters are displayed in Table I. The non-annealed sample yields a vanishing efficiency of $\eta = 0.1\,\%$, while the annealed solar cell features an efficiency of $\eta = 4.5\,\%$. In comparison to the non-annealed solar cell, the annealed one exhibits a strongly increased open circuit voltage of $V_{OC} = 485\,\mathrm{mV}$ and by four orders of magnitude reduced parasitic dark diode currents I_{01} and I_{02}. This is in accordance with Glunz,[26] where decreasing I_{01} and I_{02} led to an increase in V_{OC}. The physical origin of reduced I_{01} is, according to the two diode model, an increased charge carrier lifetime in the bulk material of the emitter or base of the solar cell and a low surface recombination velocity at the front or rear side of the solar cell.[26–29] As the laser process is applied on the front side of the solar cell, it is most likely that the bulk charge carrier lifetime in the emitter and the surface recombination velocity at the front side are affected. The physical origin of I_{02} are traps within the depletion region of the pn-junction.[26,28,29] The traps can be introduced by the laser induced damage to the silicon crystal in terms of intrinsic silicon defects or the sulfur itself.[30,31] Since I_{01} and I_{02} decrease after annealing, recombination of charge carriers and the density of traps in the space charge region are decreased.[26] While the series and parallel resistance R_s and R_p of the illuminated *IV* curve are not significantly altered by annealing, the parallel resistance from the dark *IV* curve is strongly increased after annealing, as can be seen from Table I. Obviously, the density of shunts, which are non-sensitive to illumination, decreases after the annealing process. Thus, we see the reasons for the enhanced performance of the annealed sample reduced to the following four points: (1) a lower front surface recombination velocity, (2) a higher bulk emitter carrier lifetime, (3) a lower density of traps within the space charge region, and (4) a lower density of shunts (non-sensitive to illumination). Furthermore, the efficiency of the annealed solar cell is limited by the low ($\ll 1000\,\Omega\mathrm{cm}^2$) parallel resistance and the high ($\gg 1\,\Omega\mathrm{cm}^2$) series resistance under illumination.[26] Covering the edges of the solar cell during the *IV* curve measurement and thus selecting an area of $24\,\mathrm{mm}^2$ significantly increases the parallel resistance and lowers the series resistance at illumination as shown in Fig. 1(a). Both effects increase the fill factor from $FF = 35\,\%$ to $FF = 64\,\%$ and an efficiency of $\eta = 8.2\,\%$ is achieved. We ascribe those limitations of the annealed solar cell to handling effects of the unpassivated non-sealed material creating a spatial inhomogeneity. This might be detrimental for an accurate fit with the two diode model but the huge distinction between non-annealed and annealed full size samples discloses trends and gives insight to the physical origin of obvious differences. The improvements related to the annealing as mentioned above in points (1)–(4) most likely originate from effects observed by Tull *et al.*,[18] Saring *et al.*,[19] Gimpel *et al.*,[13] and Crouch *et al.*[12] Sulfur diffusion[18] leads to segregation at intrinsic defects.[19] Therefore, some of the sulfur has the ability to saturate recombinative defects[32] and hence act as sulfur passivation. Further improvement of the material performance is based on the healing mechanism of laser induced silicon crystal lattice damages initiated by annealing.[12,13] Intrinsic silicon crystal structure changes already occur at temperatures above 400 °C.[33–35] This argument is supported by the analysis of the dark *IV* curves of Fig. 1(b). As in Hu *et al.*,[11] we determine the rectification ratio (RR) as the ratio of current at forward bias divided by the absolute value of the current at reverse bias. Thus, a high RR corresponds to a good rectification capability of the diode. At 0.9 V, the RR for the annealed sample with a value of 2680 is more than two orders higher than the value of 13 for the non-annealed sample. Furthermore, the leakage currents at −0.9 V for both kinds of samples differ by two orders of magnitude as well. The leakage current is $1.5 \times 10^{-2}\,\mathrm{mA/cm^2}$ for the annealed sample and $3.8\,\mathrm{mA/cm^2}$ for the non-annealed sample. The increase of the RR at a decrease of leakage current is ascribed by Hu *et al.*[11] to an improvement in the deformed silicon lattice. Since both effects, saturation of recombinative defects after sulfur diffusion and healed laser induced silicon crystal defects, take place within the emitter, a further characterization of the emitter is useful. Basically, the non-annealed sulfur emitter is similarly processed by Guenther *et al.*[36,37] Therefore, important data on the emitter is known

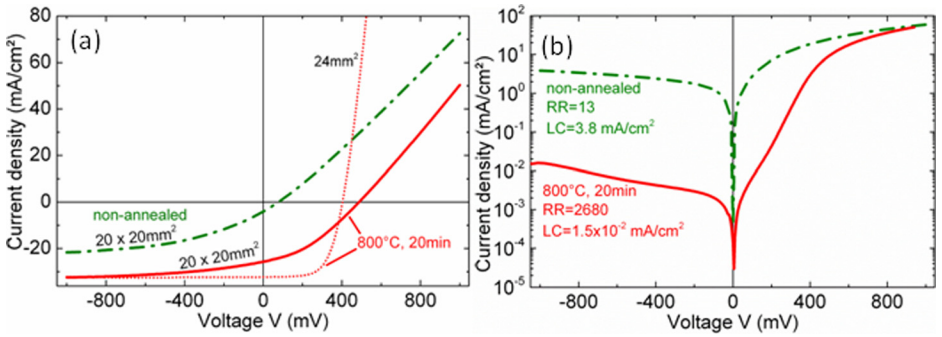

FIG. 1. (a) Illuminated and (b) dark *IV* curves of non-annealed and annealed sulfur emitter solar cells processed by femtosecond laser pulses. The main improvement in the $24\,\mathrm{mm}^2$ measurement are exhibited by $R_s = 0.9\Omega\mathrm{cm}^2$, $R_p = 3448\Omega\mathrm{cm}^2$, and $FF = 64\%$ at $\eta = 8.2\,\%$. RR is the rectification ratio and LC is the leakage current determined from dark *IV* measurements at |0.9V|.

TABLE I. *IV* curve parameters of non-annealed and annealed sulfur emitter solar cells fit with a 2 diode model via the free software IVFIT, version 2.12 (ideality factors of the first and second diode fixed at $n_1 = 1, n_2 = 2$).[25] Characteristic values from the dark *IV* curves are provided in square brackets.

Sample $20 \times 20\,mm^2$	V_{oc} (mV)	J_{sc} (mA/cm^2)	FF (%)	η (%)	R_P [darkIV] (Ω cm^2)	R_s [darkIV] (Ω cm^2)	I_{01}[darkIV] (A/cm^2)	I_{02} [darkIV] (A/ cm^2)
Non-annealed	77	4	26	0.1	51	11	8×10^{-7}	2×10^{-3}
					[333]	[15]	[4.5×10^{-7}]	[4.2×10^{-3}]
Annealed 20 min, 800 °C	485	25.8	35	4.5	101	10	6×10^{-11}	3×10^{-7}
					[126 180]	[9]	[2.2×10^{-10}]	[1.3×10^{-6}]

already: Sulfur is incorporated with a concentration of $5 \times 10^{19}\,cm^{-3}$ at its maximum near the surface, which delivers a donor level of about $1 \times 10^{17}\,cm^{-3}$, and the pn-junction is located in a depth of about $570 - 890\,nm$ for the $1 - 5\,\Omega cm$ samples[36] and $1.1\,\mu m - 2.1\,\mu m$ for samples with a boron base doping corresponding to $12 - 15\,\Omega cm$.[37] While these results cover only non-annealed samples, one would expect that by annealing due to sulfur diffusion into the bulk the sulfur concentration and the donor level slightly decreases at the surface and the junction depth may be increased. However, the corresponding values for annealed sulfur silicon would not help in clarifying the efficiency boost in the solar cell. Further insight is instead gained by looking at the emitter sheet resistance $R_{sh} \sim 1/\sigma_{Em} = 1/(e \cdot \mu_e \cdot n_e)$, where σ_{Em} is the emitter conductivity, e is the electron charge, μ_e is the electron mobility, and n_e is the charge carrier density in the emitter. R_{sh} is reciprocally proportional to μ_e and n_e and therewith allows the evaluation of contributing charge carriers in the emitter layer. We determine the emitter sheet resistance by the TLM for samples annealed at different temperatures for $t = 20\,min$ and $t = 24\,h$ as well as for samples in the non-annealed state. The sheet resistance R_{sh} is plotted versus the temperature in Fig. 2. For the non-annealed sample, $R_{sh} = 650\,\Omega/sq$. The sheet resistance increases up to $R_{sh} = 108\,k\Omega/sq$, when the annealing temperature rises to 400 °C. Above that temperature, R_{sh} decreases to $R_{sh} = 5\,k\Omega/sq$ at an annealing temperature of $T = 800\,°C$, which is still above the initial value without annealing. The wide error margin is due to the roughened surface. Accurate measurements are quite difficult, e.g., the contact area is involved in the analysis but cannot be estimated easily.[36] The increase and the subsequent decrease of R_{sh} suggest that at least two mechanisms oppose during annealing. Below 400 °C, the most likely mechanism is the diffusion of impurities. Of those impurities, we assume sulfur centers at lattice sites as the main source of donors.[32,38] The laser process induces intrinsic silicon defects, which, regarding crystallinity, entails a range from amorphous to microcrystalline silicon within the surface layer.[12,18] The dislocations and grain boundaries potentially getter diffusing impurities, in particular, sulfur.[18,19,39,40] Gettered at these defects, sulfur likely concatenates to dimers or complexes and the donor characteristics vanish. Consequently, the number of donors decreases and because $R_{sh} \sim 1/n_e$, the sheet resistance R_{sh} increases as in Fig. 2. Above 400 °C, intrinsic silicon defects can heal up by means of crystal growth.[33–35] Furthermore, as a large range of silicon crystal grain sizes is present from laser processing, some of the grains are capable to serve as nuclei or seed in our samples. Then crystal growth can occur without a long-term nucleation process.[13,33,35] The crystal quality of the emitter layer is improved and recombinative defects are reduced. The bigger the nano- and microcrystalline grains grow the higher is the electron mobility.[41,42] Thus, the charge carrier life time[40] is increased, since it is proportional to the electron mobility.[28] After all, more charge carriers contribute and the emitter sheet resistance decreases as in Fig. 2.

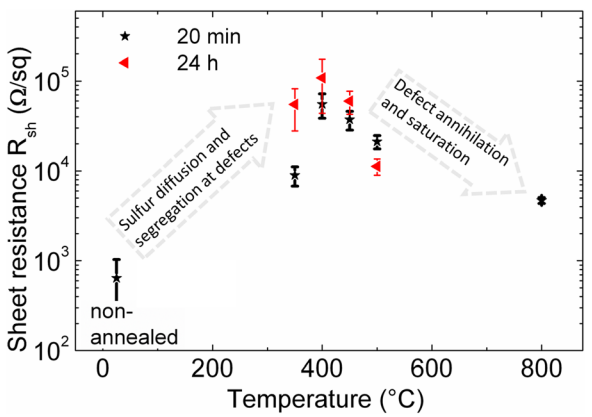

FIG. 2. Sulfur emitter sheet resistances measured by the TLM. Samples are annealed at different temperatures for 20 min and 24 h (the two arrows illustrate the influence of the underlying phenomena).

The discussed dominating mechanisms involving sulfur diffusion up to $T = 400\,°C$ and intrinsic silicon defect annihilation for higher temperatures are confirmed by annealing experiments with a duration of $t = 24\,h$. In Fig. 2, the sheet resistance of samples annealed for $t = 24\,h$ increases to a higher value of R_{sh} than for those samples with shorter annealing. This is valid up to $T = 400\,°C$. Above $T = 450\,°C$, the sheet resistance of samples annealed for $t = 24\,h$ decreases to a lower value compared to the sample annealed for $t = 20\,min$. According to Tull *et al.*,[18] the log-normal grain size distribution in the laser processed silicon is responsible for a characteristic diffusion length of sulfur. That means that sulfur diffuses a certain temperature dependent distance towards the silicon grain boundaries. As long as the sulfur remains within a silicon crystal grain during diffusion, it still might be located at silicon lattice sites, where it can act as a donor. Below 450 °C, where the emitter sheet resistance at each annealing temperature of 20 min annealed samples is lower than for 24 h annealed samples, the diffusion distance for a 20 min anneal apparently lies within the grain boundary, meaning the sulfur to be not yet at its final

position at the grain boundary, and some sulfur atoms still act as donors. For a 24 h anneal, more sulfur reaches the grain boundary, where it probably does not act as a donor. Hence, the emitter sheet resistance is higher for the 24 h annealed samples. Above 450 °C, the characteristic diffusion lengths as introduced by Tull *et al.*[18] are reached for both annealing times and the sheet resistance should be equal. However, the intrinsic silicon defect annihilation involving the rearrangement of the silicon crystal lattice is more pronounced for the 24 h anneal at 450 °C than below, and therefore more recombinative intrinsic silicon defects vanish, leaving more charge carriers, which enable a decreased emitter sheet resistance for the 24 h anneal. The sheet resistance in Fig. 2 does not reach the initial value for samples without annealing. The reason is the remaining microcrystalline silicon after annealing at $T = 800\,^{\circ}\mathrm{C}$.[12] At its grain boundaries, sulfur conglomerates bound at intrinsic defects and therewith does not contribute as a donor.[32] Nevertheless, the emitter resistance is decreased by the dominant process of silicon defect annihilation at temperatures above $T = 450\,^{\circ}\mathrm{C}$.

In conclusion, femtosecond laser sulfur hyperdoped silicon emitters in solar cells show a significant improvement after annealing at $T = 800\,^{\circ}\mathrm{C}$ for $t = 20$ min. The lowest solar cell performance, analyzed by *IV* curves, is achieved in the non-annealed state emphasizing the main losses to be recombinative defects and traps originating from the laser treatment. The sheet resistance of a sulfur emitter increases after annealing up to a temperature of 400 °C. For higher temperatures, it decreases again. Two mechanisms are responsible for this behavior: Below 400 °C, the dominant process is sulfur diffusion accumulating at intrinsic silicon defects being deactivated as donors by concatenating to dimers and complexes or by saturating intrinsic silicon defects. Above 400 °C, the probability for intrinsic laser induced silicon defects to be annihilated increases and hence the sulfur emitter sheet resistance is lowered again, however, not reaching its initial value as for the non-annealed samples. Annihilation and saturation of silicon defects reduce the number of recombination sites and traps within the depletion zone of the sulfur containing pn-junction. This effective improvement of the materials quality is demonstrated by an efficiency of more than 8 % for a solar cell featuring a femtosecond laser doped sulfur emitter.

The authors like to thank Alexander Bomm for setting up the TLM measurement and analysis tool.

[1]T. G. Kim, J. M. Warrender, and M. J. Aziz, Appl. Phys. Lett. **88**, 241902 (2006).
[2]S. H. Pan, D. Recht, S. Charnvanichborikarn, J. S. Williams, and M. J. Aziz, Appl. Phys. Lett. **98**, 121913 (2011).
[3]M. Tabbal, T. Kim, J. M. Warrender, M. J. Aziz, B. L. Cardozo, and R. S. Goldman, J. Vac. Sci. Technol. B **25**, 1847 (2007).
[4]C. H. Crouch, J. E. Carey, J. M. Warrender, M. J. Aziz, E. Mazur, and F. Y. Génin, Appl. Phys. Lett. **84**, 1850 (2004).
[5]C. Wu, C. H. Crouch, L. Zhao, J. E. Carey, R. Younkin, J. A. Levinson, E. Mazur, R. M. Farrell, P. Gothoskar, and A. Karger, Appl. Phys. Lett. **78**, 1850 (2001).
[6]J. E. Carey, C. H. Crouch, M. Y. Shen, and E. Mazur, Opt. Lett. **30**, 1773 (2005).
[7]Z. Huang, J. E. Carey, M. Liu, X. Guo, E. Mazur, and J. C. Campbell, Appl. Phys. Lett. **89**, 33506 (2006).
[8]S. Hu, P. Han, S. Wang, X. Mao, X. Li, and L. Gao, Semicond. Sci. Technol. **27**, 102002 (2012).
[9]A. J. Said, D. Recht, J. T. Sullivan, J. M. Warrender, T. Buonassisi, P. D. Persans, and M. J. Aziz, Appl. Phys. Lett. **99**, 73503 (2011).
[10]P. D. Persans, N. E. Berry, D. Recht, D. Hutchinson, H. Peterson, J. Clark, S. Charnvanichborikarn, J. S. Williams, A. DiFranzo, M. J. Aziz, and J. M. Warrender, Appl. Phys. Lett. **101**, 111105 (2012).
[11]S. Hu, P. Han, Y. Mi, Y. Xing, P. Liang, and Y. Fan, Mater. Sci. Semicond. Process. **16**, 987 (2013).
[12]C. H. Crouch, J. E. Carey, M. Shen, E. Mazur, and F. Y. Génin, Appl. Phys. A: Mater. Sci. Process. **79**, 1635–1641 (2004), see p. 1639 for diffraction rings.
[13]T. Gimpel, I. Höger, F. Falk, W. Schade, and S. Kontermann, Appl. Phys. Lett. **101**, 111911 (2012).
[14]M. T. Winkler, M.-J. Sher, Y.-T. Lin, M. J. Smith, H. Zhang, S. Gradecak, and E. Mazur, J. Appl. Phys. **111**, 93511 (2012).
[15]B. K. Newman, M.-J. Sher, E. Mazur, and T. Buonassisi, Appl. Phys. Lett. **98**, 251905 (2011).
[16]I. Umezu, J. M. Warrender, S. Charnvanichborikarn, A. Kohno, J. S. Williams, M. Tabbal, D. G. Papazoglou, X.-C. Zhang, and M. J. Aziz, J. Appl. Phys. **113**, 213501 (2013).
[17]B. K. Newman, E. Ertekin, J. T. Sullivan, M. T. Winkler, M. A. Marcus, S. C. Fakra, M.-J. Sher, E. Mazur, J. C. Grossman, and T. Buonassisi, J. Appl. Phys. **114**, 133507 (2013).
[18]B. R. Tull, M. Winkler, and E. Mazur, Appl. Phys. A: Mater. Sci. Process. **96**, 327 (2009).
[19]P. Saring, A. L. Baumann, B. Schlieper-Ludewig, S. Kontermann, W. Schade, and M. Seibt, Appl. Phys. Lett. **103**, 61904 (2013).
[20]H. H. Berger, J. Electrochem. Soc. **119**, 507 (1972).
[21]H. Berger, Solid-State Electron. **15**, 145 (1972).
[22]D. K. Schroder and D. Meier, IEEE Trans. Electron Devices **31**, 637 (1984).
[23]G. K. Reeves and H. B. Harrison, IEEE Electron Device Lett. **3**, 111 (1982).
[24]D. S. H. Chan and J. C. H. Phang, IEEE Trans. Electron Devices **34**, 286 (1987).
[25]A. R. Burgers, J. A. Eikelboom, A. Schonecker, and W. C. Sinke, in *IEEE Conference Record of the 25th IEEE PVSC* (1996), pp. 569–572.
[26]S. Glunz, PhD thesis, University of Freiburg, 1995, p. 29.
[27]A. G. Aberle, PhD thesis, University of Freiburg, 1991.
[28]M. A. Green, *Solar Cells: Operating Principles, Technology, and System Applications* (Prentice-Hall, Englewood Cliffs, NJ, 1982).
[29]A. Goetzberger, B. Voß, and J. Knobloch, *Sonnenenergie: Photovoltaik* (Teubner, 1997).
[30]E. Janzén, R. Stedman, G. Grossmann, and H. G. Grimmeiss, Phys. Rev. B **29**, 1907 (1984).
[31]H. G. Grimmeiss, E. Janzén, and B. Skarstam, J. Appl. Phys. **51**, 4212 (1980).
[32]Y. Mo, M. Z. Bazant, and E. Kaxiras, Phys. Rev. B **70**, 205210 (2004).
[33]U. Köster, Phys. Status Solidi A **48**, 313–321 (1978).
[34]M. H. Brodsky, R. S. Title, K. Weiser, and G. D. Pettit, Phys. Rev. B **1**, 2632 (1970).
[35]G. L. Olson and J. A. Roth, Mater. Sci. Rep. **3**, 1 (1988).
[36]K.-M. Guenther, T. Gimpel, S. Kontermann, and W. Schade, Appl. Phys. Lett. **102**, 202104 (2013).
[37]K.-M. Guenther, T. Gimpel, W. Schade, and S. Kontermann, in IEEE Conference Record of the 39th IEEE PVSC (2013).
[38]Y. A. Astrov, S. A. Lynch, V. B. Shuman, L. M. Portsel, A. A. Makhova, and A. N. Lodygin, Semiconductors **47**, 247–251 (2013).
[39]V. Kveder, M. Kittler, and W. Schröter, Phys. Rev. B **63**, 115208 (2001).
[40]S. Roorda, W. C. Sinke, J. M. Poate, D. C. Jacobson, S. Dierker, B. S. Dennis, D. J. Eaglesham, F. Spaepen, and P. Fuoss, Phys. Rev. B **44**, 3702 (1991).
[41]J. Y. W. Seto, J. Appl. Phys. **46**, 5247 (1975).
[42]A. Gat, L. Gerzberg, J. F. Gibbons, T. J. Magee, J. Peng, and J. D. Hong, Appl. Phys. Lett. **33**, 775 (1978).